Journal of
Mechanics of
Materials and Structures

Benjamin P. Russell, Adam Malcom, Haydn N. G. Wadley and Vikram S. Deshpande

DYNAMIC COMPRESSIVE RESPONSE OF COMPOSITE CORRUGATED CORES

BENJAMIN P. RUSSELL, ADAM MALCOM, HAYDN N. G. WADLEY AND VIKRAM S. DESHPANDE

The dynamic out-of-plane compressive response of E-glass composite corrugated sandwich cores have been measured for impact velocities ranging from quasistatic to $175\,\text{ms}^{-1}$. Laboratory scale sandwich cores of relative density $\bar{\rho} \approx 33\%$ were manufactured from 3D woven E-glass and stitched to S2-glass face-sheets via a double line of Kevlar yarn. Two variants of the sandwich cores were investigated: sandwich cores with the empty spaces between the corrugations filled with a PVC foam, and unfilled corrugations. The stresses on the rear faces of the dynamically compressed sandwich cores were measured using a direct impact Kolsky bar. The compression tests on both the corrugated cores and the parent strut wall material confirmed that these relatively high relative density corrugated cores failed by microbuckling of the strut wall material under quasistatic loading. Moreover, the foam filling did not have any significant effect on the measured responses. The peak stresses of both the strut wall material and corrugated cores increased approximately linearly with strain rate for applied strain rates less than about $4000\,\text{s}^{-1}$. This increase was attributed to the strain rate sensitivity of the composite matrix material that stabilised the microbuckling failure mode of the E-glass composite. At higher applied strain rates the response was reasonably rate insensitive with compressive crushing of the glass fibres being the dominant failure mode. A simple model utilising the measured dynamic properties of the strut wall material accurately predicts the measured peak strengths of the filled and unfilled corrugated cores.

1. Introduction

Lightweight materials and structures utilised in transportation systems are sometimes subjected to dynamic loads due to impact events or the impingement of shock waves created by nearby explosions. The development of multifunctional materials and structures that provide dynamic load mitigation capabilities in addition to their normal structural requirements are therefore important to a number of fields such as crash protection, petro-chemical safety, infrastructure protection and many military applications. There has been much interest in sandwich structures for use in dynamic loading scenarios and several theoretical and experimental studies on metallic materials have shown there to be significant advantages of sandwich structures over monolithic structures of equivalent mass, see for example [Xue and Hutchinson 2003; Fleck and Deshpande 2004; Wei et al. 2008; Dharmasena et al. 2008].

There are two effects that combine to endow sandwich panels with their superior resistance to shock front loading: (i) an increased flexural strength and (ii) fluid-structure interaction (FSI) effects, which mean that a smaller fraction of the shock impulse is transmitted into sandwich panels compared with monolithic plates of equal mass per unit area (areal density). This FSI effect for explosively created shocks in water was assessed experimentally in [Dharmasena et al. 2009; 2010]. Water shock tube

methods developed in [Deshpande et al. 2006] were used in [Mori et al. 2008] to enable the dynamic deflections of sandwich panels to be observed using Moire interferometry. The increased flexural strength of sandwich panel systems is achieved by the use of stiff, strong, fracture resistant face sheets separated by a lightweight core. Significant research is therefore underway to explore the design of lightweight sandwich panel cores that are sufficiently strong that they do not completely crush under an impulsive load.

Much of this effort in sandwich panel core design for dynamic applications has concentrated on highly ductile metallic lattice core and face sheet structures. For example, Radford et al. [2007], Ferri et al. [2006] and Tilbrook et al. [2007] have investigated the dynamic response of stainless steel square-honeycomb cores, I-cores and prismatic Y-frames and corrugated cores respectively. These studies have demonstrated that inertial stabilisation significantly delays the onset of buckling in these lattice cores; consequently, the dynamic strength exceeds the quasistatic strength by nearly a factor of four at impact velocities around $50\,\mathrm{ms}^{-1}$. Moreover, the experiments of [Radford et al. 2007] and [Tilbrook et al. 2007] have demonstrated that the peak stress on the impacted (front) face increases approximately linearly with impact velocity while the distal (rear) face stress remains approximately constant; i.e., plastic shock wave effects play a significant role at these impact velocities. These features of the dynamic compression of cellular cores results in pressure transmitted to the back face of fully back supported sandwich panels exposed to underwater shocks [Wadley et al. 2008].

There is a natural progression to adopt material systems which intrinsically have high specific strength and stiffness. Composite polymer systems reinforced with strong fibres such as carbon, glass and aramids, offer such properties. Indeed, they find extensive use within sandwich configurations in specialist automotive and aerospace markets. Some recent studies have reported the static performance of composite sandwich cores. These include an investigation of the compressive response of Z-pinned reinforced foam cores in [Marasco et al. 2006], the compressive and shear response of carbon fibre square honeycomb cores in [Russell et al. 2008], the compressive response of carbon fibre pyramidal truss cores in [Finnegan et al. 2007] and titanium coated SiC monofilaments such as those investigated in [Moongkhamklang et al. 2008]. Experimental and theoretical work on the static properties of composite corrugated cores has also been recently reported in [Kazemahvazi and Zenkert 2009] and [Kazemahvazi et al. 2009]. However, to date there is a scarcity of data in the literature on the dynamic properties of composite sandwich cores.

In this study we report the dynamic performance of composite corrugated cores. The related investigation of metallic corrugated cores in [Tilbrook et al. 2007] demonstrated that three effects give an enhanced strength to such cores under dynamic loading. These effects are: (i) material strain rate effects; (ii) inertial stabilisation of the core struts against elastic buckling and (iii) plastic shock wave effects that localise deformation near the impacted face and result in the stresses on the impacted face exceeding those on the on the face distal from the impact. However, the role that these effects play in the dynamic compression of composite corrugated cores is as yet unclear. Moreover, based on theoretical work on the dynamic compression of unidirectional composites in [Slaughter et al. 1996] and experiments in [Lankford 1995] we also anticipate that dynamic stabilisation of the microbuckling failure mode in composites will play a role in setting the dynamic performance of composite corrugated cores. We thus focus here on investigating the dynamic properties of the core material — this entails constraining the back face of the core. This boundary condition is very different from that in a sandwich plate or beam test but enables us to investigate the inherent properties of the core, absent the particular structural context.

The outline of the paper is as follows. First, the manufacturing techniques employed for making laboratory scale E-glass corrugated cores are detailed. Next, the quasistatic and dynamic out-of-plane compressive response of foam-*filled* and *unfilled* corrugated cores and the strut wall material are reported. The dynamic measurements are conducted using a direct impact Kolsky bar, and high speed photography is employed to observe the dynamic deformation modes. Based on these measurements and visual observations we finally report a simple model to relate the dynamic responses of the corrugated cores to the measured properties of the strut wall material.

2. Materials and manufacturing

Foam-filled composite corrugated sandwich cores, as sketched in Figure 1, were manufactured from 3D woven fabric (3WEAVE fabric, 3tex Inc.) and Divinycell H130 PVC foam (DIAB Inc., Desoto, TX 75115, USA). The 2.8 mm thick face sheets comprised a single layer of S2-glass (areal mass of dry fabric 3.29 kg m^{-2}) while the corrugated core was made from two layers of E-glass (areal mass of each layer 1.83 kg m^{-2}), refer to Table 1 for details of these fabrics. Each of the 3D fabric layers comprised three

	E-glass			S2-glass		
	weft (x_f)	warp (y_f)	z yarn (z_f)	weft (x_f)	warp (y_f)	z yarn (z_f)
weight	48.8%	50.3%	0.9%	48.0%	48.5%	3.6%
tows	3	2	—	3	2	—

Table 1. Details of the 3D woven glass fabrics manufactured by 3Tex: E-glass of areal mass 1.83 kg m^{-2} and S2-glass of areal mass 3.29 kg m^{-2}. The coordinate system for the fabrics is illustrated in Figure 1, right.
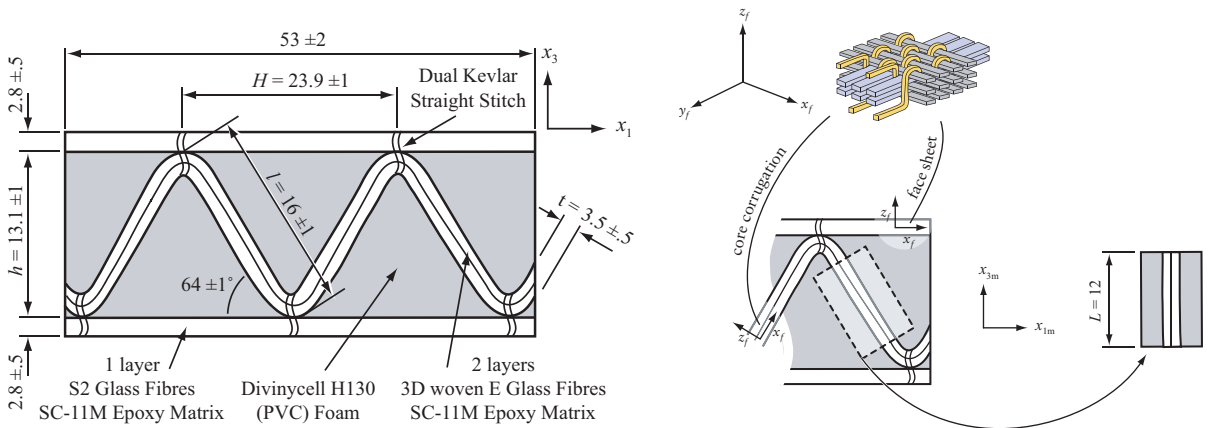

Figure 1. Left: Sketch of the corrugated core test specimens with all leading dimensions and materials used for the various components labelled. Right: Sketch illustrating the 3D fibre lay-ups in the specimens and the geometry of the test coupon used to investigate material properties of the corrugated core strut material. The coordinate systems referred to in the text are included in the figure and all dimensions are in mm.

tows in the weft direction, two tows in the warp direction and a z-yarn, all of the same fibre material. The fibre orientations in the core and face sheets are illustrated in Figure 1, right.

The corrugated core comprised struts of length $l = 16 \pm 1$ mm, thickness $t = 3.5 \pm 0.5$ mm, spaced at $H = 23.9 \pm 1$ mm. The resulting sandwich core thickness is $h = 13.1 \pm 1$ mm and has a relative density (defined here as the volume fraction of space occupied by corrugated core) $\bar{\rho} \approx 33\%$; see Figure 1, left. The variations in the dimensions are due to manufacturing variability and denote the as-measured maximum and minimum dimensions for all specimens tested in this study.

Fabrication process. The fabrication process is illustrated in Figure 2. The E-glass fabric was conformed around equilateral triangular prisms of Divinycell H130 PVC foam to form corrugations. The apexes of these corrugations were stitched to the S2-glass face sheets with Kevlar 29, size 69 thread, using a approximately 6 stitches per cm of a dual straight stitch. This whole assembly was then vacuum bagged and resin infiltrated with SC-11M epoxy (Applied Poleramic Inc., Benicia, CA 94510, USA). The SC-11M epoxy was supplied by Applied Poleramic Inc. (Benicia, California). It is a two component, two-phase (rubber toughened) system developed for shock loading applications and vacuum assisted resin transfer moulding manufacturing techniques. After mixing, the epoxy system had a viscosity of 900 cps, sufficient to permit vacuum assisted infiltration of a 500 mm × 500 mm corrugated glass core panel in 30 minutes. The panels were then cured at 72°C for 6 hours. Test specimens approximately 53 mm × 53 mm with the corrugated core arranged as shown in Figure 1, left, were then cut from these panels using a diamond cutting wheel.

In order to investigate the effect of the Divinycell foam core, specimens were also manufactured without the foam filling. Subsequently, the specimen with and without the foam filling will be referred to as the *filled* and *unfilled* specimens, respectively. In order to ensure that the unfilled specimens had the same corrugation geometry and had undergone an identical process cycle to the filled specimens, the foam filling was removed from the fully cured specimens by melting with a hot bar. This method resulted in minimal damage occurring to the corrugations and faces. The areal densities of the sandwich cores (not inclusive of faces) were 5.79 and 4.66 kg m^{-2} for the *filled* and *unfilled* geometries respectively. Additionally, sandwich specimens of the same dimensions as the corrugated cored specimens (53 mm × 53 mm) were fabricated using just the Divinycell H130 PVC foam core.

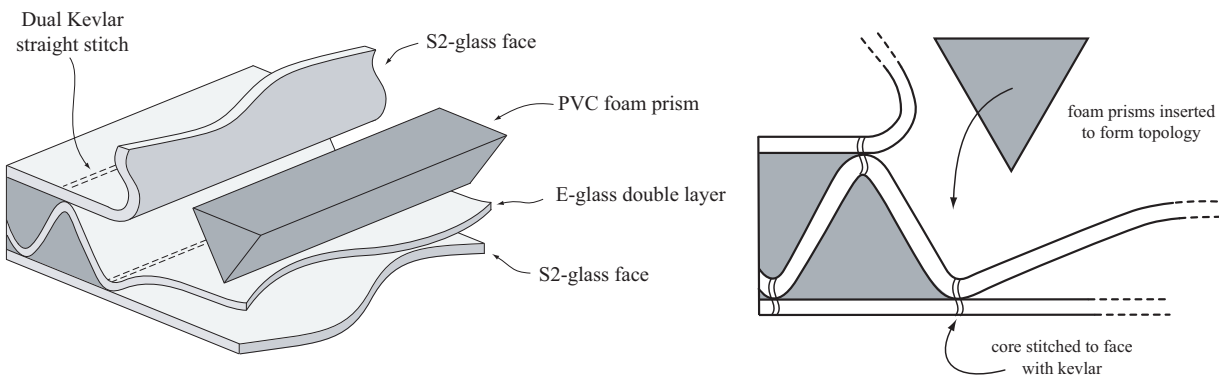**Figure 2.** Sketch of the process used to assemble the dry (uninfused) corrugated cores.

3. Experimental protocol

The quasistatic and dynamic compressive responses of the *filled* and *unfilled* corrugated cores were measured along with the corresponding compressive responses of the parent infused E-glass material comprising the struts of the corrugated core.

Specimen configurations. To measure the quasistatic and dynamic compressive responses of the infused E-glass material comprising the struts of the corrugated core, rectangular specimens of height $L = 12$ mm were cut out from the filled sandwich core as shown in Figure 1, right. These 12 mm high specimens were sufficiently stocky that under compression, Euler buckling was not the operative collapse mode and the measured responses were representative of the material rather than structural behaviours. These specimens were then compressed along the x3m direction in order to determine the axial compressive response of the strut material. As seen in the figure, some foam remained attached to the sides of the cut out rectangular specimens: since this foam had a negligible contribution to the axial compressive response of the specimen, we did not attempt to scrape it off so as to avoid any damage to the underlying composite.

The compressive tests on the sandwich specimens were conducted on the 53 mm × 53 mm sandwich specimens sketched in Figure 1, left. Initial compression experiments on these specimens exposed a failure mode that involved the breaking of the Kevlar stitches and lateral spreading of the corrugated core as shown in Figure 3a. This failure mode, while active towards the edges of a large corrugated core sandwich panel, will not be the dominant mode over the central section. We thus sought to avoid this failure mode and investigate the compressive response of the corrugated core, absent lateral spreading. This was accomplished by using the lateral steel confinement set-up as shown in Figure 3b. It is worth noting here that this confinement set-up restricted the compression of the sandwich core to a nominal compressive strain of less than 70%.

Quasistatic compression. The quasistatic compression tests were conducted in a screw-driven test machine at a nominal applied strain rate of 10^{-3} s^{-1}. The applied load was measured using the load cell of the test machine and used to obtain the applied stress while the through-thickness compressive strains
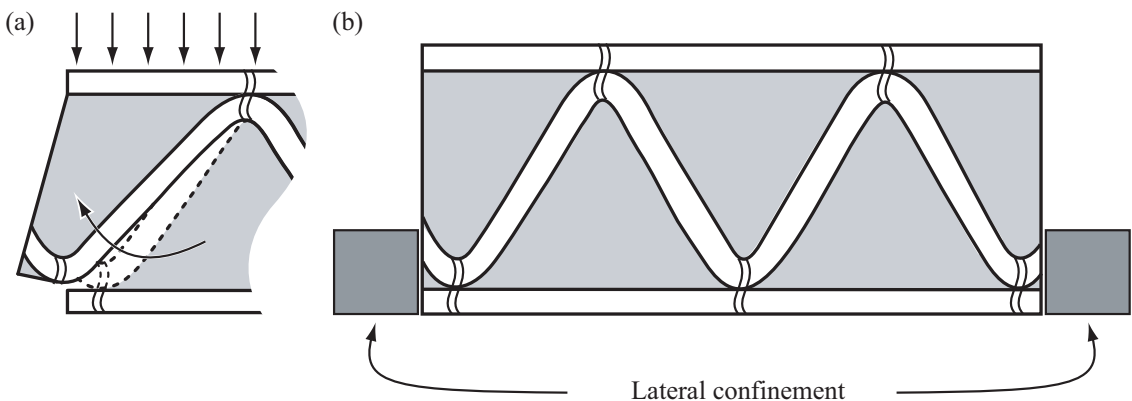

Figure 3. (a) Sketch illustrating the failure of the Kevlar stitches resulting in the lateral spreading of the corrugated core in a compression test. (b) Sketch of the lateral confinement used to prevent the failure mode illustrated in (a).

were obtained from laser extensometer measurements. Unloading-reloading cycles were also conducted in order to extract the compressive modulus of the specimens.

Dynamic compression. The dynamic out-of-plane compressive responses of the corrugated sandwich core, the strut material specimens and the H130 foam were measured from a series of direct impact tests in which the forces on the face distal from the impact were measured via a strain-gauged Kolsky bar [1949]. The specimens were placed centrally on the stationary Kolsky bar and the striker bar fired at the specimen from a gas gun as sketched in Figure 4 for the corrugated core specimens and strut material specimens respectively. The force transmitted by the specimen was measured as function of time for a range of impact velocities of the striker bar.

The kinetic energy of the projected striker governs the level of compression attained and the imposed transient velocity at the impacted end of the specimen. We wished to compress the specimens at an approximately constant velocity and chose the striker masses accordingly. It was therefore necessary to impact the samples with an initial momentum that was large compared to the change in momentum due to the dynamic resistive forces offered by the samples. The impact experiments were performed at velocities ranging from $25 \, \text{ms}^{-1}$ to $150 \, \text{ms}^{-1}$. In the experiments on sandwiches conducted at low velocity ($v_0 \leq 50 \, \text{ms}^{-1}$) a striker of mass $M = 2.5 \, \text{kg}$ was employed, while a striker of mass $M = 0.75 \, \text{kg}$ sufficed for the high velocity $v_0 > 50 \, \text{ms}^{-1}$ experiments. For the materials test, a striker of mass $M = 0.1 \, \text{kg}$ was sufficient for all velocities: high-speed photographs taken during these experiments confirm that these striker masses are sufficient to provide almost constant velocity compression for nominal compressive strains of up to 40%.

The striker was given the required velocity by firing it from a gas gun of barrel length of 4.5 m. No sabot was employed as the cylindrical strikers had a diameter equal to the inner diameter of the gun
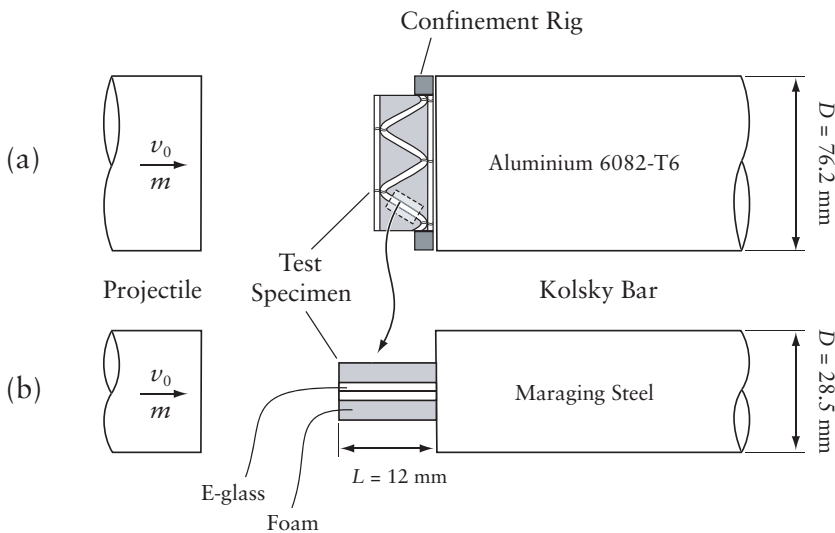

Figure 4. Sketches of the Kolsky bar setup arrangements for dynamic testing of the (a) corrugated core specimens and (b) the E-glass test coupons cut from the struts of the corrugated cores.

barrel and also equal to the diameter of the Kolsky bar. The bursting of copper shim diaphragms formed the breech mechanism of the gun. The impact experiments were performed at velocities ranging from approximately $10\,\mathrm{ms}^{-1}$ to $150\,\mathrm{ms}^{-1}$. The velocity of the projectile was measured at the exit of the barrel using laser-velocity gates and the impacted end of the Kolsky bar was placed $100\,\mathrm{mm}$ from the open end of the gun barrel.

The set-up of the Kolsky pressure bar is standard. A circular cylindrical bar of length $2.0\,\mathrm{m}$ was used. The pressure history on the impacted end of the bar was measured by diametrically opposed axial strain gauges placed approximately 10 diameters from the impact end of the bar. The elastic strain histories in the bars were monitored using the two $120\,\Omega$ TML foil gauges of gauge length $1\,\mathrm{mm}$ in a half-Wheatstone bridge configuration. A strain bridge amplifier of cut-off frequency $500\,\mathrm{kHz}$ was used to provide the bridge input voltage and a digital storage oscilloscope was used to record the output signal. The bridge system was calibrated dynamically over the range of strains measured during the experiments and was accurate to within 3%. Two separate Kolsky bars were used for testing the corrugated core specimens and the material test coupons (Figure 1, right), as follows:

(i) a $76.2\,\mathrm{mm}$ diameter bar from aluminium alloy (AL-P6082T6, yield strength $310\,\mathrm{MPa}$) was used in the corrugated core tests, while

(ii) a $28.5\,\mathrm{mm}$, diameter bar from maraging steel (yield strength exceeding $1000\,\mathrm{MPa}$) was used in the material coupon tests.

These two different diameter bars were used so as to ensure that the difference between the cross-sectional areas of the specimens and the Kolsky bars were kept to a practical minimum. The longitudinal elastic wave speed was measured at $5092\,\mathrm{ms}^{-1}$ in the aluminium alloy bar, and $4906\,\mathrm{ms}^{-1}$ in the maraging steel bar. Taking into account that the strain gauges are placed approximately 10 bar diameters from the impacted end, this gives a time-window of $487\,\mu\mathrm{s}$ and $781\,\mu\mathrm{s}$ in the aluminium and steel Kolsky bars, respectively before elastic reflections from the distal end of the bar complicated the measurement of stress.

The response time and accuracy of the measurement system were gauged from a series of calibration tests. We report the result of one such representative test on the maraging steel Kolsky bar. A maraging steel striker of diameter $28.4\,\mathrm{mm}$ and length $460\,\mathrm{mm}$ was fired at the Kolsky bar at a velocity $v_0 = 6.6\,\mathrm{ms}^{-1}$. The measured stress versus time response measured by the strain gauges on the Kolsky bar is plotted in Fig.5. With time $t = 0$ corresponding to the instant of impact, the stress pulse arrives at the gauge location at $t = 58\,\mu\mathrm{s}$. Elastic wave theory predicts that the axial stress in the bar is $\rho c v_0/2 = 131\,\mathrm{MPa}$, where ρ and c are the density and longitudinal elastic wave speed of steel respectively. The measured peak value of the stress is within 1% of this prediction. However, the measurement system has a finite response time, with the stress rising to this peak value in approximately $13\,\mu\mathrm{s}$ (see the insert in Figure 5). This rise time places an operational limit on measuring the dynamic response of the specimens. It becomes significant at the higher velocities because significant compression of the specimen is achieved within the first $5\,\mu\mathrm{s}$. The measured stress in the calibration test drops back to zero at $t = 273\,\mu\mathrm{s}$; due to the reflection of the elastic wave from the distal end of the striker bar.

In a number of the experiments, high-speed photographic sequences were taken using a Phantom V12 camera, thereby allowing observation of the deformation process.
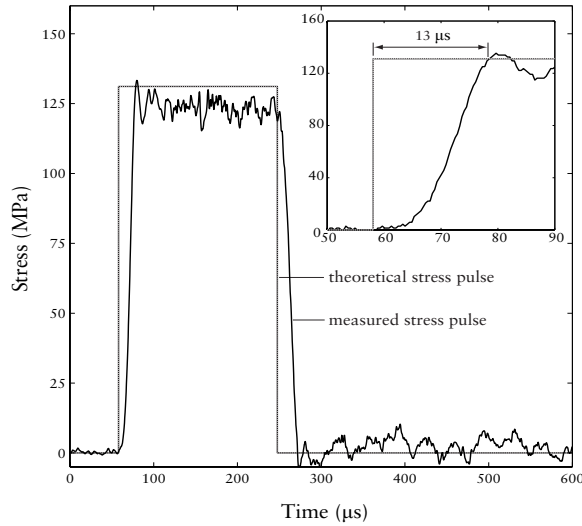
Figure 5. Stress versus time history measured in the $D = 28.5$ mm maraging steel Kolsky bar during a calibration test in which a 460 mm long steel striker ($D = 28.5$ mm) was fired at the Kolsky bar at $v_0 = 6.6$ ms^{-1}. The theoretical prediction based on 1D elastic wave theory is included, along with a magnified graph of the stress pulse's onset.

4. Quasistatic response

The measured compressive responses of the corrugated core strut wall material are plotted in Figure 6, left. The material test coupons were compressed along the x_{3m} direction (refer to Figure 1, right), which corresponds to the x_f fibre direction of the fabric. Results from three repeat tests are shown to indicate
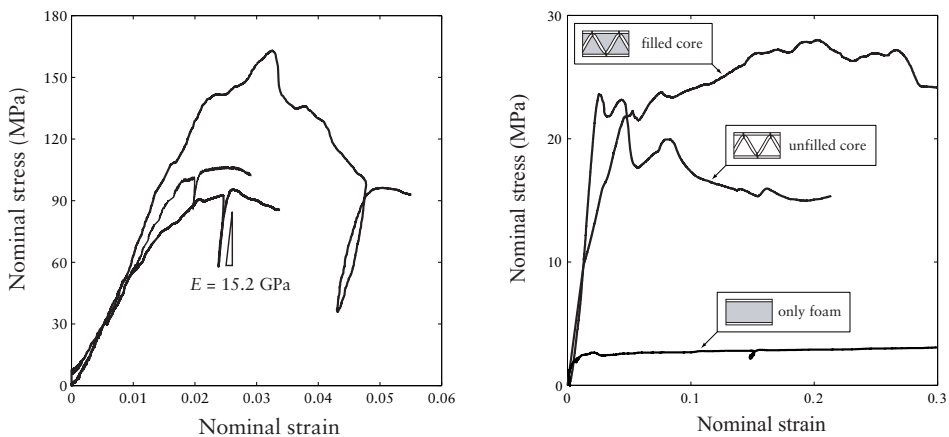
Figure 6. The measured quasistatic stress versus strain responses of the E-glass composites comprising the struts of the corrugated cores (left) and the filled, unfilled corrugated cores and the H130 Divinycell foam cores (right). The compressive response of the E-glass composite was measured along the x_f direction (see Figure 1, right).

the variability in the measured responses: this scatter is mainly a result of manufacturing variability that resulted in variations in the amount of infused matrix from specimen to specimen. The average measured peak strength was approximately $\sigma_s = 100$ MPa while the compressive modulus of the specimens was determined to be about Es = 15 GPa. Photographs of two representative deformed specimens at a nominal compressive strain of approximately 3% are shown in Figure 7a: a clear microbuckle is visible, confirming that the peak strength measured in these quasistatic experiments is set by the microbuckling strength of the E-glass composites.

Measurements of the quasistatic compressive responses of the *filled* and *unfilled* corrugated cores are plotted in Figure 6, right, along with the compressive response of the H130 Divinycell foam. Following an initial linear elastic response, a nonlinear response sets in at about 22 MPa and 23 MPa for the *filled* and *unfilled* cores respectively. However, while the *unfilled* core then displays a softening response the *filled* core exhibits a moderate hardening. The H130 foam is much weaker than the corrugated cores with a plateau strength around 2.5 MPa.

A montage of photographs showing the deformation of the *filled* and *unfilled* corrugated cores is included in Figure 7b. The first microbuckle develops in both cores at a compressive strain of about 3% and is reminiscent of the microbuckle observed in the compressive test performed on the strut wall material (Figure 7a). This suggests that the onset of nonlinearity in the compressive responses of the cores
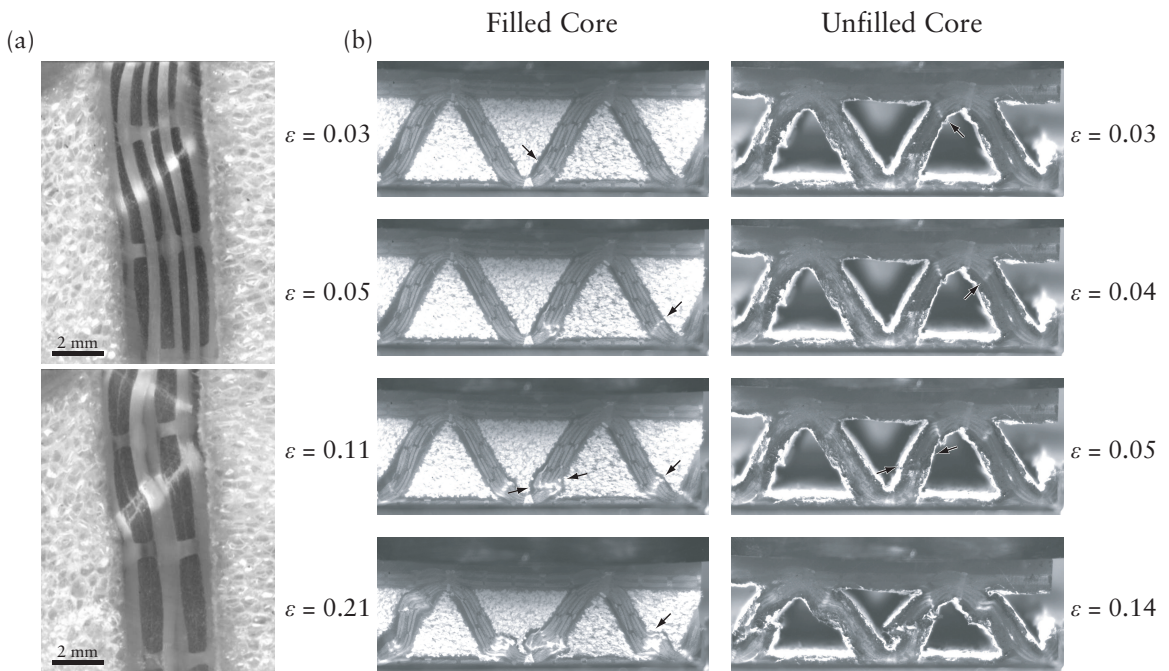

Figure 7. (a) Two representative photographs (at a compressive strain of about 3%) showing the microbuckle failure of the E-glass composite during the quasistatic compression of the test coupons. (b) A montage of photographs showing the sequences of deformation during the quasistatic compression of the filled and unfilled corrugated core test specimens.

is a result of the microbuckling of the E-glass composite material. Additional microbuckles subsequently appear in adjacent struts and the struts then begin to shear over. This shearing process is impeded by the H130 foam in the *filled* core which results in the mild hardening observed in Figure 6, right. By contrast, the shearing of the *unfilled* core is unimpeded, resulting in a softening response after the onset of microbuckling in the struts.

The peak strength σ_p of the *unfilled* corrugated core is expected to be set by either the Euler buckling or microbuckling of the struts and given in terms of the core geometry and strut wall material properties by [Côté et al. 2006]

$$\sigma_p = \begin{cases} \dfrac{\pi^2}{6}\left(\dfrac{t}{l}\right)^3 \dfrac{h}{H} E_s & \text{if } \dfrac{\sigma_s}{E_s} > \dfrac{\pi^2}{12}\left(\dfrac{t}{l}\right)^2, \\ 2\dfrac{t}{l}\dfrac{h}{H}\sigma_s, & \text{otherwise.} \end{cases} \tag{1}$$

This expression clearly shows that the peak strength of the corrugated core investigated here is set by the microbuckling of the struts. Note that this does not involve any modelling of the microbuckle stress σ_s itself but rather takes as an input, the experimentally measured value. Inserting the strut geometry and material parameters in (1) predicts that $\sigma_p = 24$ MPa and is in good agreement with the measurements.

Foam support is expected to enhance the Euler buckling strength of the struts of the corrugated core [Cartié and Fleck 2003]. Given that the strength of the unfilled corrugated core is set by the microbuckling strength of the E-glass composite struts, it is not surprising that the initial "yield" strength is unaffected by the foam filling we anticipate that the peak strength of an E-glass corrugated core with significantly more slender struts (i.e., lower relative density) will be enhanced with a foam filling.

5. Dynamic response

Strut wall material. The measured dynamic compressive responses of the $L = 12$ mm high E-glass specimens cut from the strut walls is plotted in Figure 8, left, for impact velocities in the range $25\,\text{ms}^{-1} \leq v_0 \leq 150\,\text{ms}^{-1}$. In the figures the compressive responses are plotted in terms of the nominal stress as measured at the distal end of the specimen (i.e., the nonimpacted end of the specimen) versus the applied nominal strain $v_0 t/L$, where t is the time measured after the initiation of deformation. The measured peak stress σ_f is seen to increase from about 200 MPa for $v_0 = 25\,\text{ms}^{-1}$ to 400 MPa at $v_0 = 150\,\text{ms}^{-1}$. It is worth noting here that the peak stress is achieved at $t \approx 12\,\mu\text{s}$ for $v_0 \geq 50\,\text{ms}^{-1}$: this time is approximately equal to the response time of the Kolsky bar apparatus (see Figure 5) and thus while the peak stress measurements reported here are accurate, the data cannot be used to extract the dynamic modulus of the E-glass composite.

Given the measured Young's modulus E_s and the density ($2550\,\text{kg m}^{-3}$) of the E-glass composite, we anticipate that the longitudinal elastic wave speed for the E-glass composite is approximately $4000\,\text{ms}^{-1}$. Thus, within the $12\,\mu\text{s}$ required to achieve peak stress, about 4 elastic reflections take place in the $L = 12$ mm specimen. It is therefore reasonable to assume that the specimen is in axial equilibrium at the instant that the peak stress is measured, and that the measured peak strength is a material property independent of the specimen dimensions. Given this, we summarise the measured peak strengths σ_f as a function of the applied nominal strain rate $\dot{\epsilon} \equiv v_0/L$ in Figure 8, right. The measurements are well-fitted by a bilinear curve with the peak strength increasing linearly with strain rate for $\dot{\epsilon} \leq 4000\,\text{s}^{-1}$ and reasonably rate-independent at higher values of $\dot{\epsilon}$.
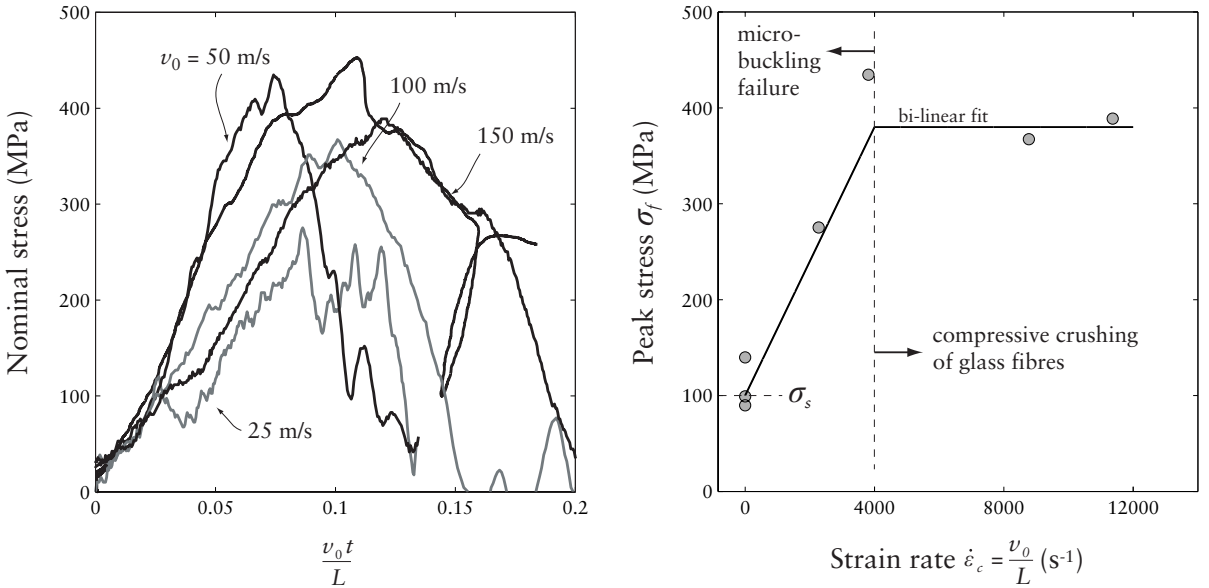
Figure 8. Left: The measured dynamic stress versus nominal strain responses of the E-glass material coupons for a range of impact velocities. Right: Summary of the measured peak stresses E-glass specimens as a function of applied strain rate. The compressive response of the E-glass composite was measured along the x_f direction (see Figure 1, right).

Recall that the peak strength under quasistatic loading is set by the microbuckling failure stress. Increasing the applied strain rate results in stabilisation of the microbuckle failure mode resulting in the peak strength increasing with $\dot{\epsilon}$. This stabilisation can be due to either (i) inertial stabilisation of the buckling or (ii) matrix strain rate effects. Theoretical work by Fan and Slaughter [1997] suggests that inertial effects become significant for strain rates greater than about $4000\,\mathrm{s}^{-1}$. We therefore expect that this measured rate sensitivity is due to matrix strain rate effects. The increase in the microbuckling strength due to matrix strain rate effects can be understood as follows. An approximate expression for the microbuckling strength in terms of the matrix shear strength τ_y is, according to [Argon 1972],

$$\sigma_c = \frac{\tau_y}{\bar{\phi}}, \tag{2}$$

where $\bar{\phi}$ is the fibre misalignment angle. Thus, the enhanced matrix shear strength at higher strain rates is expected to also increase the microbuckling strength σ_c. The measurements indicate that the measured peak strength rises to a maximum of about $400\,\mathrm{MPa}$. This maximum peak strength is not set by microbuckling of the fibres but rather by the compressive crush strength of glass fibres. This is rationalised as follows. The volume fraction of fibres in the direction of the loading is about 20%, which implies that the corresponding fibre stress is about $2\,\mathrm{GPa}$ [CES 2009]. This is equal to the compressive crush strength of glass, confirming that the maximum compressive strength of the E-glass composites at high strain rates is governed by the compressive crush strength of the constituent glass fibres.
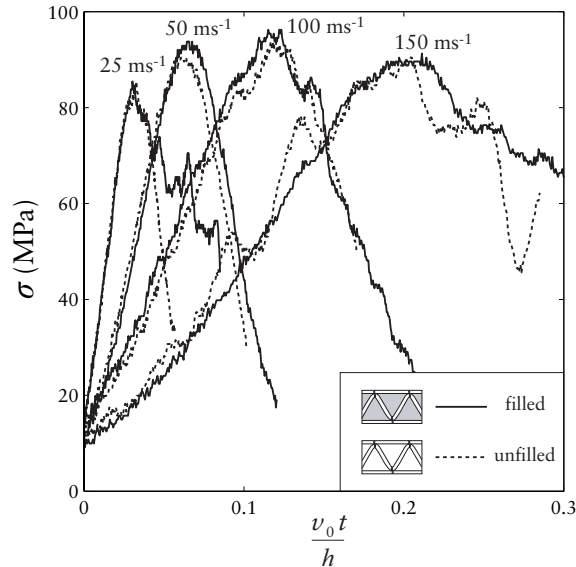
Figure 9. The measured dynamic stress versus nominal strain responses of the filled and unfilled corrugated core specimens. The stresses are measured on the rear faces of the specimen distal from the impacted face.

Corrugated cores. The measured dynamic compressive responses of the *filled* and *unfilled* corrugated cores are plotted in Figure 9 using axes of the compressive stress σ versus nominal strain $v_0 t / h$, where time t = 0 corresponds to the instant that the striker bar impacts the specimen. Recall that the stress σ is measured on the rear face of the specimen distal from the impacted face. The responses of the *filled* and *unfilled* specimens are almost identical with the measured peak stress of approximately 90 MPa over the velocity range $25 \, \text{ms}^{-1} \leq v_0 \leq 175 \, \text{ms}^{-1}$. Again we note that the peak stress is observed to occur at time t in the range $15 \, \mu\text{s} - 18 \, \mu\text{s}$. This is similar to the response time of the Kolsky bar apparatus (Figure 5) and so these measurements again cannot be used to infer the dynamic compressive moduli of the specimens.

Montages showing the sequence of deformation of the *filled* and *unfilled* corrugated cores impacted at $v_0 = 50 \, \text{ms}^{-1}$ and $150 \, \text{ms}^{-1}$ are included in Figures 10 and 11, respectively. While the deformation modes of the corrugated cores impacted at $50 \, \text{ms}^{-1}$ look similar to those observed under quasistatic deformation (Figure 7b), a marked difference is seen when $v_0 = 150 \, \text{ms}^{-1}$. At this high velocity, deformation is more localised near the impacted face with the corrugated core "stubbing" against the impacted face. This deformation mode was also observed in metallic corrugated cores by [Tilbrook et al. 2007]. Given this highly localised deformation near the impacted face we anticipate that the stresses on the impacted face are higher than the stresses measured at the distal end, i.e., the specimen is not in axial equilibrium in line with the finite element calculations of [Tilbrook et al. 2007]. These differences between the stresses on the impacted and distal surfaces cannot be measured in this direct Kolsky bar set-up as the inertia of the impacted face-sheet dominates the measurements; see [Tilbrook et al. 2007] for further discussion. We emphasise that this localised deformation mode was observed only for $v_0 \geq 150 \, \text{ms}^{-1}$; at the lower impact
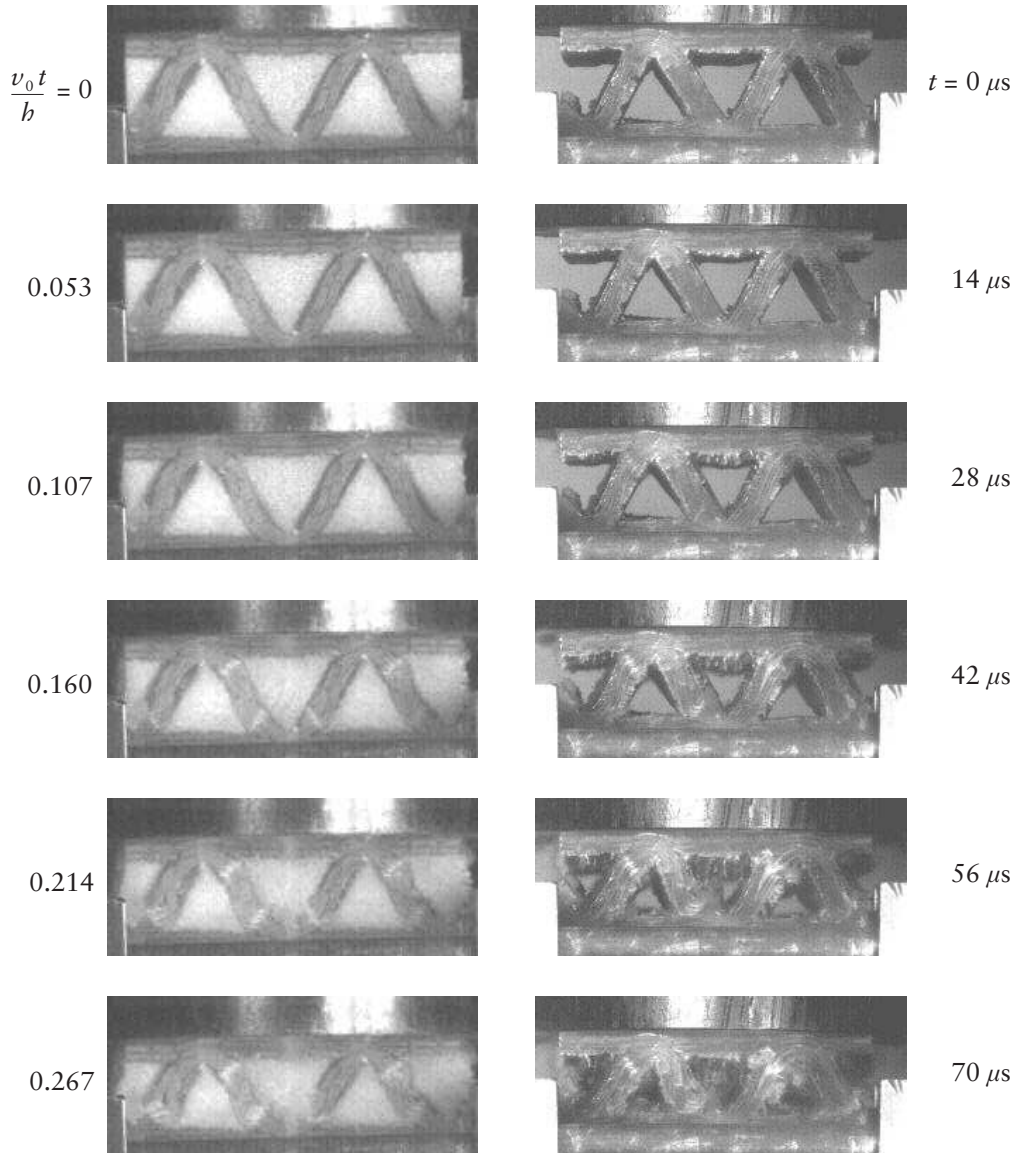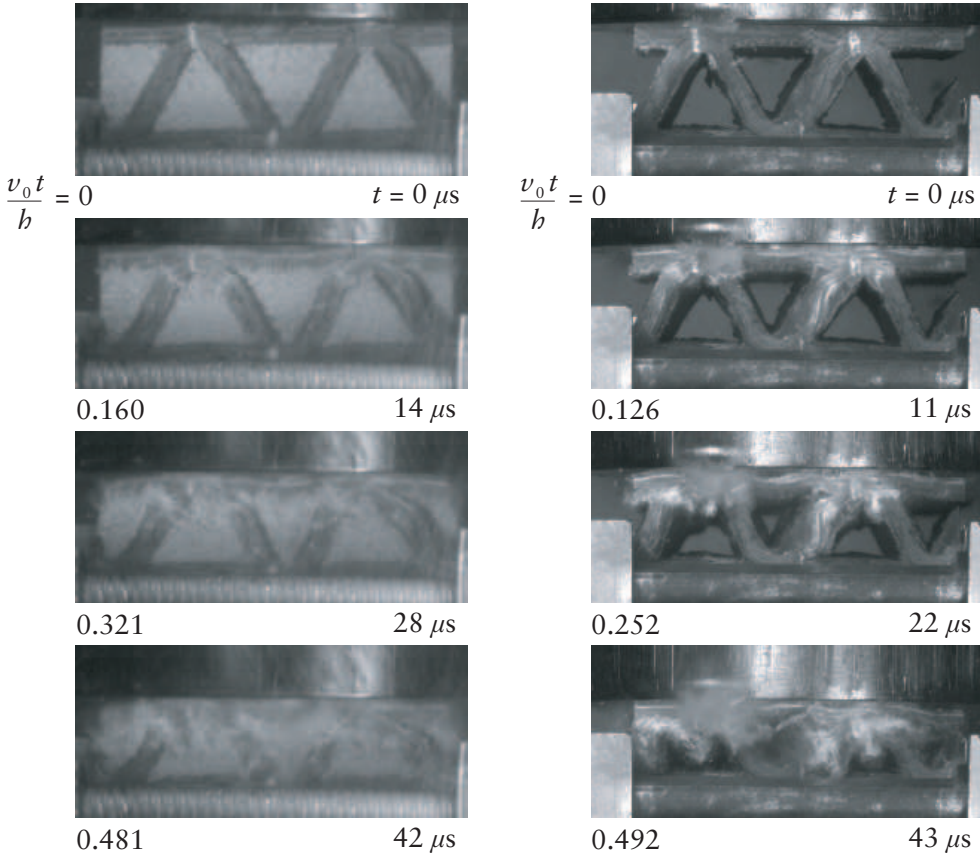
Figure 10. Deformation sequences in the filled (left) and unfilled (right) corrugated core specimens impacted at a velocity $v_0 = 50\,\text{ms}^{-1}$. Impact occurs on the top face of the specimens in the photographs.

velocities the deformation was reasonably uniform through the core, suggesting that the specimens were in axial equilibrium at lower impact velocities.

The measured peak stresses on the rear face of the filled and unfilled corrugated cores specimens (i.e., distal from the impacted face) are plotted in Figure 12 as a function of the impact velocity v_0 and applied strain rate $\dot{\epsilon}_c \equiv v_0/h$ (upper scale). The dependence of the peak strengths of the corrugated cores on strain rate is similar to the parent strut wall material (Figure 8, right), with the peak stress increasing with strain

Figure 11. Deformation sequences in the filled (left) and unfilled (right) corrugated core specimens impacted at a velocity $v_0 = 150 \, \text{ms}^{-1}$. Impact occurs on the top face of the specimens in the photographs.

rate for $\dot{\epsilon}_c < 4000 \, \text{s}^{-1}$ and being reasonably rate insensitive at higher values of $\dot{\epsilon}_c$. This clearly indicates that there exist two regimes of deformation: (i) microbuckling of the strut wall for $\dot{\epsilon}_c < 4000 \, \text{s}^{-1}$ and (ii) compressive crushing of the glass fibres at higher strain rates. We proceed to report a simplified analysis for relating the peak strengths of the corrugated cores to the measured E-glass properties (Figure 8, right). This is made possible by the fact that (i) Euler buckling is not the operative failure mode over the entire range of impact velocities investigated here and (ii) except at the highest impact velocity ($v_0 \geq 150 \, \text{ms}^{-1}$) the specimens are in axial equilibrium. The peak strength of the corrugated core as a function of the applied strain rate $\dot{\epsilon}_c$ is then specified from (1) as

$$\sigma_P(\dot{\epsilon}_c) = 2\left(\frac{t}{l}\right)\left(\frac{h}{H}\right)\sigma_f(\dot{\epsilon}), \quad \text{where } \dot{\epsilon} = \dot{\epsilon}_c\left(\frac{h}{l}\right)^2. \tag{3}$$

The strut material strength as a function of strain rate, $\sigma_f(\dot{\epsilon})$, is given in Figure 8, right. The predictions of Equation (3) are plotted in Figure 12. Two bounds on the predictions are shown based on the measured variations of the specimen dimensions (Figure 1, left). These predictions adequately bound the measured
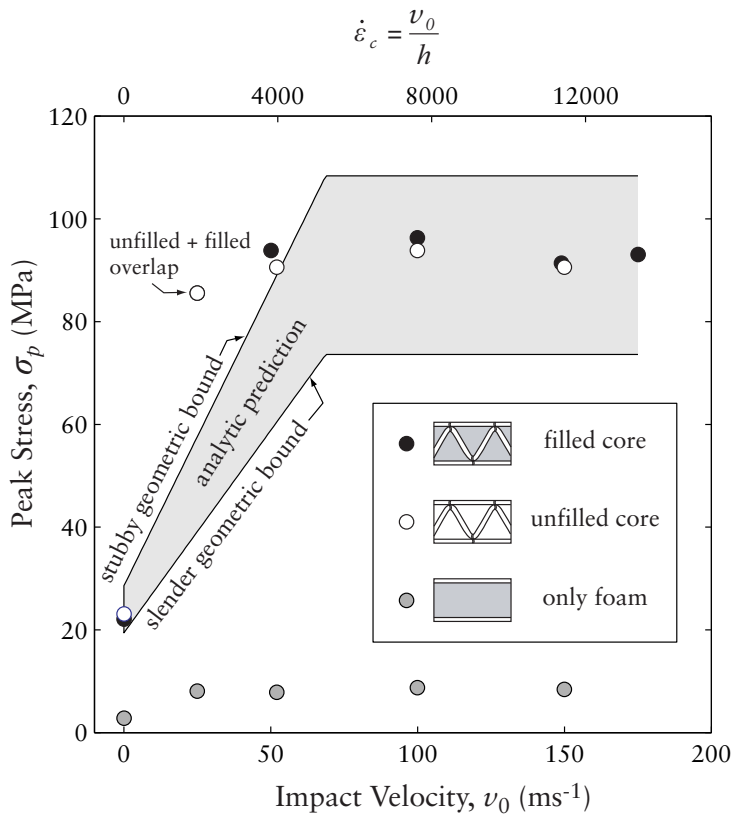
Figure 12. Summary of the measured peak stresses in the filled and unfilled corrugated core specimens as function of the impact velocity (lower x-axis) and applied nominal strain rate (upper x-axis). The measured peak stresses in the H130 Divinycell foam are also included.

dynamic peak strengths of the *filled* and *unfilled* corrugated cores, indicating that over the range of impact velocities investigated here, the strain rate sensitivity of the high relative density corrugated cores is governed by the rate sensitivity of the parent strut wall material and is not significantly affected by inertial stabilisation against elastic buckling as observed in the low relative density metallic corrugated cores investigated by [Tilbrook et al. 2007]. The exceptions are data points at $25\,\mathrm{ms}^{-1}$, that fall outside of the bounds of the analytical prediction. The discrepancy here is attributed to the simplicity of the model which assumes an empirically based bilinear relationship of strength with strain rate which is not expected to be accurate near the transition in the strain rate response.

Recall that in the present study, the struts of the corrugated core are sufficiently stubby as to not fail by Euler buckling, even under quasistatic loading. This meant that the dynamic tests were unable to reveal strength enhancements due to microinertial effects but rather only displayed strength enhancements due to material strain rate effects. Tests on corrugated cores with significantly more slender struts would enable us to investigate the microinertial effects in composite cores: current manufacturing methods preclude this at present but this is suggested as a topic for future investigation.

6. Concluding remarks

E-glass corrugated sandwich cores of relative density $\bar{\rho} \approx 33\%$ were manufactured by wrapping 3D woven E-glass fabric over triangular prismatic PVC foam inserts and then stitching the assembly to S2-glass face sheets. The entire assembly was then infused with an epoxy resin. The foam inserts were scraped out of some of the specimens and the dynamic out-of-plane compressive stresses on the rear faces of the *filled* and *unfilled* corrugated core specimens measured at impact velocities ranging from quasistatic to $175 \, \text{ms}^{-1}$ using a direct impact Kolsky bar.

The corrugated cores had stubby struts and failed by microbuckling of these struts under quasistatic compression. The foam filling had only a minor effect, stabilising the postpeak strut failure response of the corrugated core. Under dynamic loading, the deformation of the specimens was reasonably uniform through the core thickness for impact velocities less than about $150 \, \text{ms}^{-1}$; at higher impact velocities deformation was localised near the impacted face, suggesting that the specimens were not in axial equilibrium and shock effects came into play. Foam filling had nearly no effect on the measured dynamic properties of the corrugated cores with the peak stresses of both the strut wall material and corrugated cores increasing approximately linearly with strain rate for applied strain rates less than about $4000 \, \text{s}^{-1}$. This increase was attributed to the strain rate sensitivity of the composite matrix that stabilised the microbuckling failure mode of the E-glass composite. At higher applied strain rates the response was reasonably rate insensitive with compressive crushing of the glass fibres being the dominant failure mode. A simple model utilising the measured dynamic properties of the strut wall material accurately predicts the measured peak strengths of the *filled* and *unfilled* corrugated cores.

References

[Argon 1972] A. S. Argon, "Fracture of composites", *Treatise Mater. Sci. Technol.* **1** (1972), 79–114.

[Cartié and Fleck 2003] D. D. Cartié and N. A. Fleck, "The effect of pin reinforcement upon the through-thickness compressive strength of foam-cored sandwich panels", *Compos. Sci. Technol.* **63**:16 (2003), 2401–2409.

[CES 2009] "CES Materials Selector Database", *Granta Design Limited, UK* (2009).

[Côté et al. 2006] F. Côté, V. S. Deshpande, N. A. Fleck, and A. G. Evans, "The compressive and shear responses of corrugated and diamond lattice materials", *Int. J. Solids Struct.* **43**:20 (2006), 6220–6242.

[Deshpande et al. 2006] V. S. Deshpande, A. Heaver, and N. A. Fleck, "An underwater shock simulator", *Proc. R. Soc. Lond. A* **462**:2067 (2006), 1021–1041.

[Dharmasena et al. 2008] K. P. Dharmasena, H. N. G. Wadley, Z. Y. Xue, and J. W. Hutchinson, "Mechanical response of metallic honeycomb sandwich panel structures to high-intensity dynamic loading", *Int. J. Impact Eng.* **35**:9 (2008), 1063–1074.

[Dharmasena et al. 2009] K. Dharmasena, D. Queheillalt, H. Wadley, Y. Chen, P. Dudt, D. Knight, Z. Wei, and A. Evans, "Dynamic response of a multilayer prismatic structure to impulsive loads incident from water", *Int. J. Impact Eng.* **36**:4 (2009), 632–643.

[Dharmasena et al. 2010] K. P. Dharmasena, D. T. Queheillalt, H. N. G. Wadley, P. Dudt, Y. Chen, D. Knight, A. G. Evans, and V. S. Deshpande, "Dynamic compression of metallic sandwich structures during planar impulsive loading in water", *Eur. J. Mech. A Solids* **29**:1 (2010), 56–67.

[Fan and Slaughter 1997] J. Q. Fan and W. S. Slaughter, "High strain rate compression of fiber composites", *J. Mech. Phys. Solids* **45**:5 (1997), 731–751.

[Ferri et al. 2006] E. Ferri, E. Antinucci, M. Y. He, J. W. Hutchinson, F. W. Zok, and A. G. Evans, "Dynamic buckling of impulsively loaded prismatic cores", *J. Mech. Mater. Struct.* **1**:8 (2006), 1345–1365.

[Finnegan et al. 2007] K. Finnegan, G. Kooistra, H. N. G. Wadley, and V. S. Deshpande, "The compressive response of carbon fiber composite pyramidal truss sandwich cores", *Int. J. Mater. Res. Z. Metallkd.* 12 (2007), 1264–1272.

[Fleck and Deshpande 2004] N. A. Fleck and V. S. Deshpande, "The resistance of clamped sandwich beams to shock loading", *J. Appl. Mech.* (*ASME*) **71**:3 (2004), 386–401.

[Kazemahvazi and Zenkert 2009] S. Kazemahvazi and D. Zenkert, "Corrugated all-composite sandwich structures, I: modeling", *Compos. Sci. Technol.* **69**:7–8 (2009), 913–919.

[Kazemahvazi et al. 2009] S. Kazemahvazi, D. Tanner, and D. Zenkert, "Corrugated all-composite sandwich structures, II: failure mechanisms and experimental programme", *Compos. Sci. Technol.* **69**:7–8 (2009), 920–925.

[Kolsky 1949] H. Kolsky, "An investigation of the mechanical properties of materials at very high rates of loading", *Proc. Phys. Soc. B* **62**:11 (1949), 676–700.

[Lankford 1995] J. Lankford, "The failure of fiber-reinforced ceramic-matrix composites under dynamic loading", *JOM* **47**:5 (1995), 64–68.

[Marasco et al. 2006] A. I. Marasco, D. D. R. Cartié, I. K. Partridge, and A. Rezai, "Mechanical properties balance in novel Z-pinned sandwich panels: out-of-plane properties", *Compos. A Appl. Sci. Manuf.* **37**:2 (2006), 295–302.

[Moongkhamklang et al. 2008] P. Moongkhamklang, D. M. Elzey, and H. N. G. Wadley, "Titanium matrix composite lattice structures", *Compos. A Appl. Sci. Manuf.* **39**:2 (2008), 176–187.

[Mori et al. 2008] L. F. Mori, D. T. Queheillalt, H. N. G. Wadley, and H. D. Espinosa, "Deformation and failure modes of i-core sandwich structures subjected to underwater impulsive loads", *Exp. Mech.* **49**:2 (2008), 257–275.

[Radford et al. 2007] D. D. Radford, G. J. McShane, V. S. Deshpande, and N. A. Fleck, "Dynamic compressive response of stainless-steel square honeycombs", *J. Appl. Mech.* (*ASME*) **74**:4 (2007), 658–67.

[Russell et al. 2008] B. P. Russell, V. S. Deshpande, and H. N. G. Wadley, "Quasistatic deformation and failure modes of composite square honeycombs", *J. Mech. Mater. Struct.* **3**:7 (2008), 1315–1340.

[Slaughter et al. 1996] W. S. Slaughter, J. Q. Fan, and N. A. Fleck, "Dynamic compressive failure of fiber composites", *J. Mech. Phys. Solids* **44**:11 (1996), 1867–1890.

[Tilbrook et al. 2007] M. T. Tilbrook, D. D. Radford, V. S. Deshpande, and N. A. Fleck, "Dynamic crushing of sandwich panels with prismatic lattice cores", *Int. J. Solids Struct.* **44**:18–19 (2007), 6101–6123.

[Wadley et al. 2008] H. Wadley, K. Dharmasena, Y. C. Chen, P. Dudt, D. Knight, R. Charette, and K. Kiddy, "Compressive response of multilayered pyramidal lattices during underwater shock loading", *Int. J. Impact Eng.* **35**:9 (2008), 1102–1114.

[Wei et al. 2008] Z. Wei, V. S. Deshpande, A. G. Evans, K. P. Dharmasena, D. T. Queheillalt, H. N. G. Wadley, Y. V. Murty, R. K. Elzey, P. Dudt, Y. Chen, D. Knight, and K. Kiddy, "The resistance of metallic plates to localized impulse", *J. Mech. Phys. Solids* **56**:5 (2008), 2074–2091.

[Xue and Hutchinson 2003] Z. Y. Xue and J. W. Hutchinson, "Preliminary assessment of sandwich plates subject to blast loads", *Int. J. Mech. Sci.* **45**:4 (2003), 687–705.

BENJAMIN P. RUSSELL: bpr23@cam.ac.uk
University of Cambridge, Engineering Department, Trumpington Street, Cambridge, CB2 1PZ, United Kingdom

ADAM MALCOM: am4uz@virginia.edu
University of Virginia, Department of Materials Science and Engineering, Charlottesville, VA 22904, United States

HAYDN N. G. WADLEY: haydn@virginia.edu
University of Virginia, Department of Materials Science and Engineering, Charlottesville, VA 22904, United States

VIKRAM S. DESHPANDE: vsd@eng.cam.ac.uk
University of Cambridge, Engineering Department, Trumpington Street, Cambridge, CB2 1PZ, United Kingdom

JOURNAL OF MECHANICS OF MATERIALS AND STRUCTURES

http://www.jomms.org

Founded by Charles R. Steele and Marie-Louise Steele

Cover design: Alex Scorpan

See inside back cover or http://www.jomms.org for submission guidelines.

Journal of Mechanics of Materials and Structures